Journal of Inorganic and Organometallic Polymers and Materials
https://doi.org/10.1007/s10904-025-03838-w

RESEARCH

First Principles Study of the Properties of Cs_2GaAgF_6 Double Halide Perovskite Compound for Optoelectronic and Thermoelectric Applications

Mwende Mbilo[1] · Robinson Musembi[1] · John Peter Kachira[1,2] · Martin Nyamunga[1] · Ibrahim Musanyi[1] · Samuel Wafula[1] · Madallah Yusuf[3]

Received: 19 February 2025 / Accepted: 1 May 2025

Abstract

This study uses first-principles methods to analyze the structural, electronic, mechanical, thermophysical, optical, and thermoelectric properties of the Cs_2GaAgF_6 double-halide perovskite compound. The results have revealed that the Cs_2GaAgF_6 compound is mechanically and thermodynamically stable and can be potentially synthesized. The calculated band gap of the material was 2.27 eV, 2.41 eV, and 2.54 eV, derived from the local density approximation using Perdew–Zunger functional (LDA-PZ), the generalized gradient approximation using the Wu–Cohen (GGA-WC), and Perdew–Burke–Ernzerhof (GGA-PBE) functionals, respectively. The band gap was improved by using metaGGA functionals, which gave 3.10 eV, 3.15 eV, 3.15 eV, and 4.62 eV for strongly constrained and appropriately normed (SCAN), regularized strongly constrained and appropriately normed (rSCAN), restored-regularized strongly constrained and appropriately normed (r2SCAN), and Tran–Blaha-modified Becke–Johnson (TB-mBJ), respectively. The machine learning (ML) techniques predicted a band gap of 2.68 eV. The mechanical and elastic properties showed that the investigated compound is ductile and elastically anisotropic. Additionally, the optical properties showed excellent performance in the ultraviolet spectrum. Notably, the high absorption coefficients and optical conductivity values across the ultraviolet spectrum underscore the significant potential of the Cs_2GaAgF_6 double-halide perovskite compound for optoelectronic applications. Finally, the Cs_2GaAgF_6 double-halide perovskite compound showed a considerable figure of merit (ZT) value of 0.739 at approximately 600 K, suggesting its suitability for thermoelectric applications.

Keywords Double-halide perovskite · DFT · Thermodynamic stability · Optoelectronics · Thermoelectric applications

1 Introduction

As global energy demand continues to increase with industrial growth and social development, excessive reliance on traditional fossil fuels poses significant challenges, particularly considering escalating ecological concerns [1]. Modern society's unprecedented energy needs have intensified environmental degradation owing to pollution from the byproducts of high-carbon energy use. This growing pressure highlights the urgent need to transition to non-fossil energy sources, steering the world toward a low-carbon future.

Photovoltaics have attracted immense attention as non-fossil energy sources owing to the global abundance of sunlight [2]. Silicon-based photovoltaics have proven to be ideal candidates for non-fossil photovoltaic sources

✉ Mwende Mbilo
mwendebilo@gmail.com

1 Monolith Research Group, Department of Physics, Faculty of Science and Technology, University of Nairobi, P.O. Box 30197, 00100 Nairobi, Kenya

2 Department of Physics, Mbeya University of Science and Technology, P.O. Box 131, Mbeya, Tanzania

3 Computational and Theoretical Physics Group (CTheP), Department of Physical Sciences, Kaimosi Friends University, P.O. Box 385-50309, Kaimosi, Kenya

Published online: 08 July 2025

because of their advanced technology and high efficiency [3]. Since the theoretical efficiency limit for crystalline silicon photovoltaics is 29.4%, only marginal performance improvements are possible due to intrinsic losses and Auger recombination [4]. Researchers are increasingly focusing on perovskite solar cells (PSCs) as an emerging technology that can deliver high power conversion efficiency (PCE) [5] while maintaining low production costs [6]. PSCs have made remarkable advancements over the past few decades, particularly in their PCE, which has surged to 26.7% [7]. This leap in efficiency has been achieved primarily through the use of lead-based perovskite compounds. However, reliance on lead presents significant environmental and health risks, raising concerns regarding the sustainability of PSC technology [8]. Lead is a toxic metal that can pose serious hazards if not managed properly, particularly in the manufacturing and disposal of solar panels. As the quest for higher efficiencies continues, it is crucial to address these challenges by exploring alternative materials that could replace lead in perovskite formulations while still achieving comparable efficiency.

Lead-free double-halide perovskites, represented by the formula $A_2BB'X_6$, have attracted significant research interest owing to their remarkable properties [9]. Effective perovskite materials have been developed by substituting Pb^{2+} ions with a combination of monovalent B^{+} and trivalent B'^{3+} cations [10]. Charef et al. [9] investigated the properties of Na_2AgAsX_6 (X = Cl, Br) double-halide perovskite materials using the first-principles method. The desirable band gaps, high absorption in the ultraviolet and visible regions, and good transport properties from this investigation highlighted the potential of these double-halide perovskites as light absorbers for efficient PSCs and thermoelectric applications. The Rb_2AgGaX_6 (X: Br, Cl) double-halide perovskites [11] have been found to exhibit band gaps of 1.28 and 2.53 eV and high absorption coefficients of 1.9×10^5 cm^{-1} and 2.1×10^5 cm^{-1}, desirable for energy applications. The PCEs of Rb_2AgGaX_6 (X: Br, Cl) were simulated theoretically under AM 1.5G solar irradiation to be 32.2 and 12%, respectively, further proving their potential for solar-cell device design. Double-halide perovskite compounds A_2AgAsX_6 (A = K, Rb, Cs; X = Cl, Br, I) based on arsenic were found to have band gaps ranging from 0.882 to 2.125 eV using the first-principles method [12]. These compounds also exhibited high absorption coefficients in the ultraviolet-visible region, indicating their potential for energy applications.

Double-halide perovskite compounds with Gallium and Silver combinations ($Cs_2AgGa(Cl, Br)_6$) have been studied for optoelectronic and thermoelectric applications using density functional theory (DFT) [13]. Electronic band gaps of about 2.57 eV and 1.42 eV were obtained for $Cs_2AgGaCl_6$ and $Cs_2AgGaBr_6$, respectively. Both compounds exhibited high absorption coefficients (10^5 cm^{-1}) in the ultraviolet and visible regions. A perovskite solar cell based on $Cs_2AgGaBr_6$ was modeled and achieved a high PCE of 32.57%. This shows the potential of Gallium and Silver combinations for realizing efficient double-halide perovskite devices.

The highest reported experimental PCE for lead-free double-halide perovskite solar cells is 6.37% [14]. This was achieved using hydrogenated Cs–AgBiBr perovskite materials. This efficiency is much lower than that achieved using lead-based perovskite materials. Therefore, it is necessary to explore double-halide perovskite materials further to bridge this efficiency gap. In addition, fluoride-based double-halide perovskites have been under-investigated in the literature compared to their iodine, chlorine, and bromine counterparts. Based on the above, we propose a fluoride-based double-halide perovskite compound with a Gallium and Silver combination. No theoretical and experimental studies on the properties of the Cs_2GaAgF_6 material have been reported in the literature, which motivates this study. In particular, a systematic DFT study of the structural, electronic, elastic, mechanical, optical, and thermoelectric properties of Cs_2GaAgF_6 double-halide perovskite compound was conducted using local and semi-local functionals for optoelectronic and thermoelectric applications.

2 Computational Methods

In this investigation, the structural, electronic, elastic, mechanical, optical, and thermoelectric properties of the Cs_2GaAgF_6 double-halide perovskite compound were computed using the plane wave self-consistent field PWscf method in the framework of density functional theory (DFT) [15], as implemented in the Quantum Espresso (QE) code [16]. Ultrasoft pseudopotentials (USPP) [17] and norm-conserving pseudopotentials (NCPP) [18] have been employed to describe the interactions between electrons and ions. USPP was utilized to predict the structural, electronic, elastic, mechanical, and thermoelectric properties, whereas NCPP was used to predict the optical properties. This study employs local and semi-local approximations. These include the local density approximation (LDA) [19] and the generalized gradient approximation (GGA), utilizing the Perdew–Zunger (PZ), Perdew–Burke–Ernzerhof (PBE) [20], and Wu–Cohen (WC) [21] functional schemes to account for exchange-correlation effects. The strongly constrained and appropriately normed (SCAN), regularized strongly constrained and appropriately normed (rSCAN), restored-regularized strongly constrained and appropriately normed (r2SCAN) [22, 23, 24], and Tran–Blaha-modified Becke–Johnson (TB-mBJ) [25] functionals were further

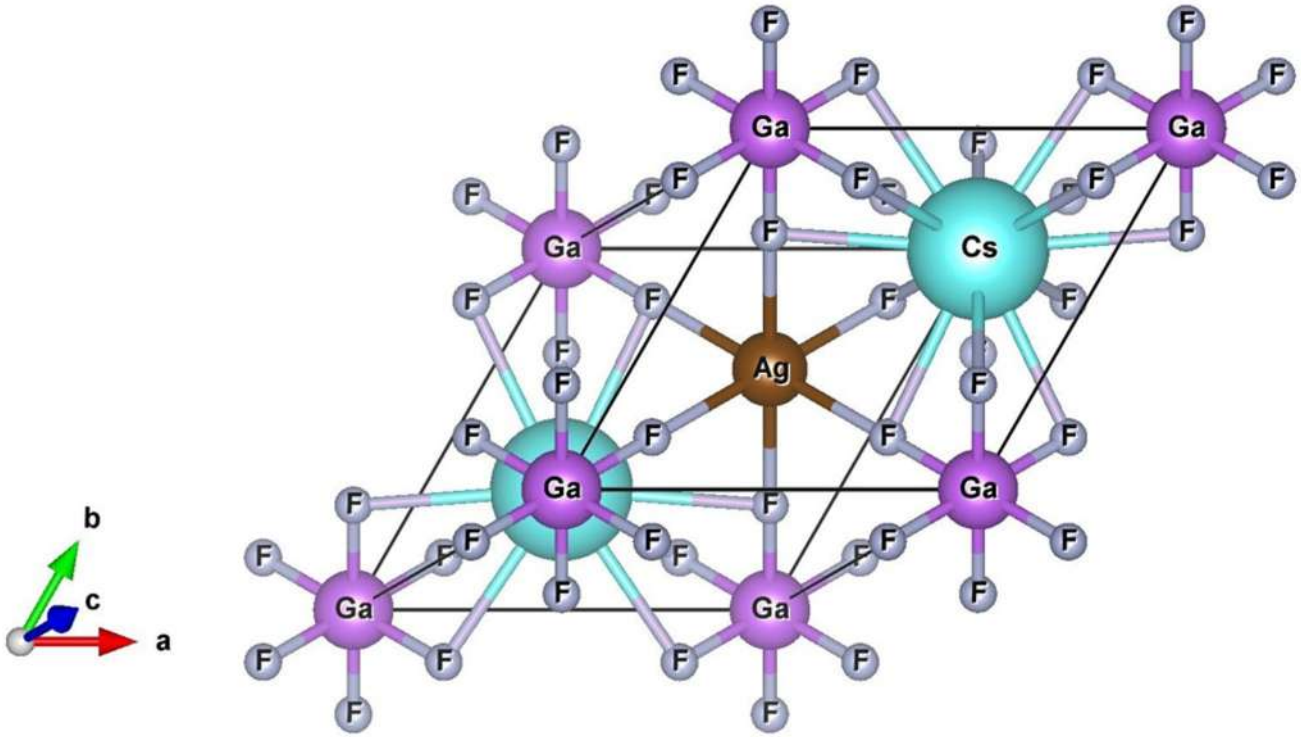

Fig. 1 Primitive crystal structure of Cs_2GaAgF_6 double-halide perovskite compound

Table 1 Ground state structural properties of Cs $_2$GaAgF$_6$ double-halide perovskite compound

	GGA-PBE	GGA-WC	LDA
Lattice parameter a_0 (Å)	9.025	8.850	8.654
Bulk modulus B_0 (GPa)	13.97	15.90	18.79
Equilibrium volume V_0 (Å^3)	734.91	693.75	647.42
Energy of formation ΔHf (Ry)	− 1.77	− 1.78	− 1.88

used to improve the accuracy of the band gaps because LDA and GGA tend to underestimate them [26, 27]. Other than DFT, the aflow machine learning online tool (AFLOW-ML) accessed at www.aflowlib.org was used to predict the band gap of the Cs_2GaAgF_6 double-halide perovskite compound. The authors of the ML model and its accuracy and error margins are reported in the literature [28, 29, 30, 31]. The first irreducible Brillouin Zone sampling was performed using a Monkhorst–Pack sampling scheme with a converged k-point grid set at 9 × 9 × 9 with a 1 offset. A converged kinetic energy cutoff of 150 Rydberg and a charge density cutoff of 1200 Rydberg were applied for the calculations. A denser k-point grid of 12 × 12 × 12 was used for the non-self-consistent field calculations. A geometry optimization step was performed to calculate the ground-state structural properties. This was achieved by minimizing the total energy with respect to the cell dimensions, followed by fitting these values to the Birch-Murnaghan equation of state [32] to obtain the ground-state crystal structure parameters. Further optimization was done through the variable cell relaxation to relax the atoms by employing the Broyden–Fletcher–Goldfarb–Shanno (BFGS) algorithm. The crystal structure of Cs_2GaAgF_6 was visualized using VESTA software. All other electronic, elastic, mechanical, optical, and thermoelectric properties were predicted under the optimized conditions.

3 Results and Discussion

3.1 Structural Properties

The Cs_2GaAgF_6 double-halide perovskite compound crystallizes in a cubic structure with the Fm−3m (225) space group [33]. Figure 1 shows the primitive crystal structure. The Cs atoms are bonded to twelve equivalent F atoms to form a Cs–F bond with a length of 3.18 Å, Ag is bonded to six equivalent F atoms to form an Ag–F bond with a length of 2.53 Å, whereas Ga is bonded to six equivalent F atoms to form a Ga–F bond with a length of 1.94 Å.

The geometry optimization of the total energy versus different unit cell volumes results in values that are fitted into the Birch-Murnaghan equation of state [32] to determine the ground-state structural properties, which are presented in Table 1. Using both LDA and GGA, the value of the equilibrium lattice parameter, $a_{0,}$ ranged from 8.654 to 9.025 Å.

The bulk modulus describes the resistance against changes in volume due to the applied external pressure [34]. A large bulk modulus indicates a hard material. The computed B_o values using the GGA and LDA methods range between 13.97 and 18.79 GPa. Compared with the bulk moduli of representative soft materials ($NaSbS_2$ polymorphs) of 20.60 GPa [35], Cs_2GaAgF_6 demonstrates a slightly lower bulk modulus, placing it as a relatively soft material.

The energy of formation (ΔH_f) was calculated using Eq. (1) [36].

$$\Delta H_f = E_{\mathrm{Cs2GaAgF6}} - (2E_{\mathrm{Cs}} + \mathrm{E_{Ga}} + E_{\mathrm{Ag}} + 6E_{\mathrm{F}}) \quad (1)$$

where $E_{\mathrm{Cs2GaAgF6}}$ is the total energy of Cs $_2$GaAgF$_6$ double-halide perovskite compound while E_{Cs}, E_{Ga}, E_{Ag}, and E_{F} are total energies of isolated Cs, Ga, Ag, and F atoms, respectively.

The values of ΔH_f calculated using both local and semi-local functionals were negative, indicating that the Cs_2GaAgF_6 double-halide perovskite compound is thermodynamically stable [36]. Further, the dynamic stability of the Cs_2GaAgF_6 double-halide perovskite compound was studied by computing phonon dispersions. This was performed using a linear response method based on perturbation density functional theory (DFPT) [37], in which the force constants, interatomic dynamical matrices, and the lattice dynamics are determined from the nuclear geometry and electronic charges [37]. The thermos_pw code of Quantum Espresso, and a q-points grid of 4×4×4 in the crystal lattice, was used for phonon dispersion calculations. As observed in Fig. 2, the phonon dispersion curve of the Cs_2GaAgF_6 double-halide perovskite compound has positive frequency modes, proving its dynamical stability [38]. The thermodynamic stability of the Cs_2GaAgF_6 compound indicates its potential synthesizability. While no experimental synthesis was attempted in this work, similar wide band gap double-halide perovskites such as [Cs_2XBiCl_6 (X=Al, Ag) [39, 40] have been successfully synthesized, supporting the feasibility of synthesizing Cs_2GaAgF_6 under suitable conditions.

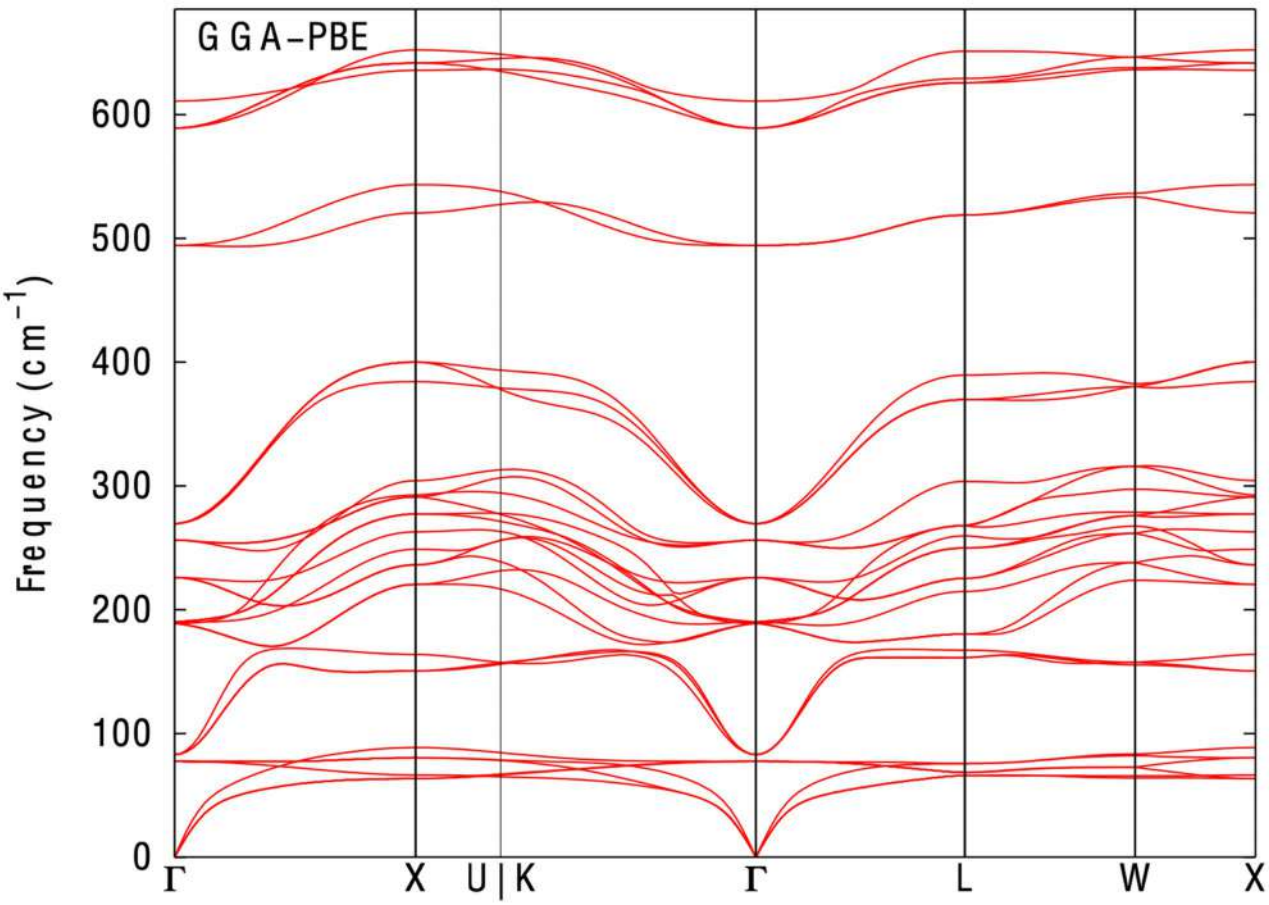

Fig. 2 Phonon dispersion curve of Cs_2GaAgF_6 double-halide perovskite compound

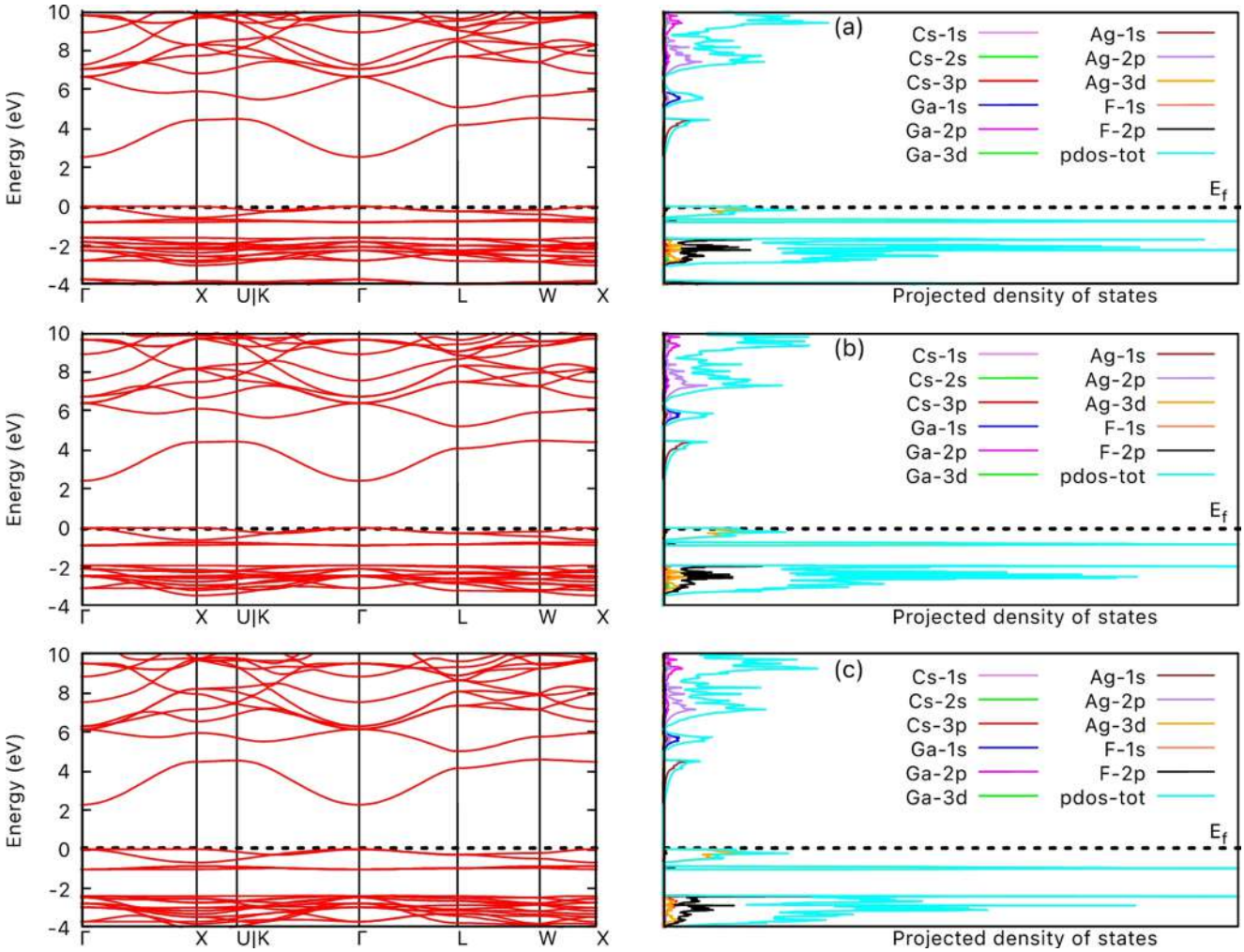

Fig. 3 The band structure and projected density of states of the Cs_2GaAgF_6 double-halide perovskite compound computed using **a** GGA-PBE, **b** GGA-WC, and **c** LDA approximations

3.2 Electronic Properties

The electronic band structure and projected density of states are effective for determining the nature of a material. An overlap of the electronic states in the valence and conduction bands at the Fermi level implies that the material under investigation is a conductor; otherwise, it is a semiconductor [41]. The electronic states in Fig. 3 show a separation gap between the valence and conduction bands, suggesting that the Cs_2GaAgF_6 double-halide perovskite compound is a semiconductor. The valence band maxima and the conduction band minima lie on the same/different high symmetry points, Γ–Γ and X–Γ, in the first Brillouin zone, implying that the Cs_2GaAgF_6 double-halide perovskite compound is a direct/indirect band gap semiconductor [42]. Figure 3 shows that the Cs_2GaAgF_6 double-halide perovskite compound has wide band gaps of 2.54, 2.41, and 2.27 eV using GGA-PBE, GGA-WC, and LDA approximations. LDA and GGA approximations are known to understate the electronic band gaps of semiconducting materials [41]. Therefore, the SCAN, RSCAN, R2SCAN, and TB-mBJ functionals were utilized to improve accuracy. As shown in Table 2, the band gap of the Cs_2GaAgF_6 double-halide perovskite compound increased to 3.1, 3.15, 3.15, and 4.62 eV by utilizing the SCAN, RSCAN, R2SCAN, and TB-mBJ functionals,

Table 2 The electronic band gaps of the Cs_2GaAgF_6 double-halide perovskite compound calculated using different approximations

Methods	Band gaps (eV)
GGA-PBE	2.54
GGA-WC	2.41
LDA	2.27
SCAN	3.10
RSCAN	3.15
R2SCAN	3.15
TB-mBJ	4.62
AFLOW-ML	2.68

respectively. These wide band gap values are closely related to the ones reported for other double-halide perovskite compounds ($Cs_2AgGaCl_6$, Cs_2NaXCl_6 (X=In, La, Sc, Y), Rb_2NaTlZ_6 (Z=Cl, Br, and I), and Cs_2YAgX_6 (X=Cl, Br, I)) with similar stoichiometry [13, 43, 44, 45]. The AFLOW-ML tool predicted the band gap of the Cs_2GaAgF_6 double-halide perovskite compound to be 2.68 eV. This value is closely related to the values obtained from DFT methods, suggesting the reliability of DFT methods in predicting electronic band gaps. The wide band gaps obtained for the Cs_2GaAgF_6 semiconductor material render it suitable for optoelectronic applications [46]. It was further observed from the projected density of states in Fig. 3 that the F2*p* and Ag3*d* states dominated the formation of the valence band. In contrast, the Ga2*p*, Ag2*p*, Ga1*s*, and Ag1*s* states significantly contributed to the formation of the conduction band. All other unaccounted states contributed insignificantly to the formation of the valence and conduction bands.

3.3 Elastic and Mechanical Properties

The elastic properties/constants (Cij) of the Cs_2GaAgF_6 compound were computed using the thermos_pw code in Quantum Espresso. The cubic crystal system features three independent elastic constants, namely C_{11}, C_{12}, and C_{44} [47]. The Born stability criteria for the cubic crystal system are $C_{11}-C_{12}>0$, $C_{11}+2C_{12}>0$, and $C_{44}>0$ [47]. The computed elastic constants for the Cs_2GaAgF_6 double-halide perovskite compound adhere to the mentioned Born stability criteria, symbolizing mechanical stability. From these elastic constants, other mechanical properties, including bulk modulus B, Young's modulus E, Shear modulus G, and Poisson's ratio *v*, are deduced using the Voigt-Reuss-Hill (VRH) averaging scheme [48]. The Voigt and Reuss constants are represented by Eqs. (2) and (3), while the Hill's average of the Voigt and Reuss schemes for a cubic crystal system is given by Eq. (4) [49].

$$B_V = \frac{(C_{11}+2C_{12})}{3}; \quad G_V = \frac{(C_{11}-C_{12}+3C_{44})}{5} \tag{2}$$

Table 3 The elastic constants in GPa and mechanical properties of the Cs_2GaAgF_6 cubic crystal structure

	GGA-PBE
C11	45.56
C12	35.47
C44	16.08
B (GPa)	38.83
E (GPa)	27.89
G (GPa)	10.12
B/G	3.84
v	0.38
A	3.19

$$B_V = B_R; \quad G_R = \frac{5\,(C_{11}-C_{12})\,C_{44}}{4C_{44}+3\,(C_{11}-C_{12})} \tag{3}$$

$$B = \frac{B_V+B_R}{2}; \quad G = \frac{G_V+G_R}{2} \tag{4}$$

The Young's modulus and Poisson's ratio are calculated using Eq. (5).

$$E = \frac{9BG}{3B+G}; \quad \nu = \frac{3B-2G}{2(3B=G)} \tag{5}$$

The B, E, and G describe the ability of a material to resist volume deformation, uniaxial tension, and plastic deformation, respectively [50]. The B/G and *v* ratio investigates the materials' ductile and brittle nature. A B/G ratio greater than 1.75 denotes a ductile nature; otherwise, a brittle nature [51]. Moreover, a material is said to be brittle if $v<0.26$ and ductile if $v>0.26$ [51]. The obtained B/G and *v* values in Table 3 show that the Cs_2GaAgF_6 double-halide perovskite compound exhibits a ductile nature. The elastic anisotropy (A) in cubic crystal systems is characterized by Eq. (6) [52]. The A value of 1 demonstrates that a material is elastically isotropic; any deviations prove anisotropy. Our calculations indicate that the Cs_2GaAgF_6 double-halide perovskite compound is elastically anisotropic.

$$A = \frac{2C_{44}}{C_{11}-C_{12}} \tag{6}$$

To further estimate the mechanical anisotropy of the Cs_2GaAgF_6 compound, the 3D spatial dependences of the Young's modulus and Shear modulus along the x, y, and z planes were deduced from the elastic constants using the ELATE: Elastic matrix tensor analysis [53] software, as shown in Fig. 4. A material is termed isotropic if the 3D distribution maps adopt a spherical shape; otherwise, it is anisotropic [54]. According to Fig. 4, the distribution maps show a deviation from the spherical shape, suggesting anisotropic behavior.

3.4 Optical Properties

To determine the potential application of the Cs_2GaAgF_6 double-halide perovskite compound in optoelectronics, its optical properties were investigated by computing the complex dielectric wave function. The GGA-PBE approximation was used as a representative method to compute the complex dielectric wave function. The complex dielectric wave function describes the electron response in a material and is represented by Eq. (7) [55, 56].

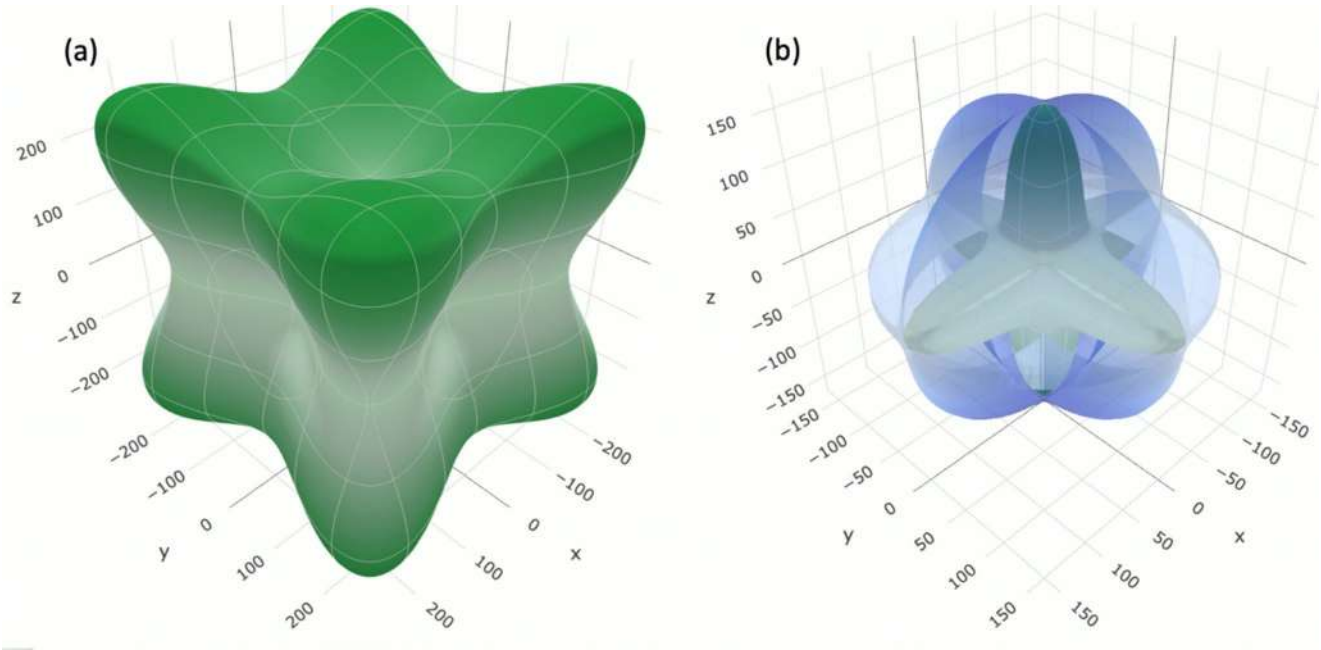

Fig. 4 Three-dimensional distribution maps of **a** Young's modulus and **b** shear modulus of Cs_2GaAgF_6 lead-free double perovskite compound along the x, y, and z planes

$$\epsilon(\omega) = \epsilon_1(\omega) + i\epsilon_2(\omega) \tag{7}$$

where $\varepsilon_1(\omega)$ and $\varepsilon_2(\omega)$ are the real and imaginary components of the dielectric wave function. The other optical properties, such as the refractive index n(ω), absorption coefficient α(ω), optical conductivity σ(ω), extinction coefficient K(ω), reflectivity R(ω), and energy loss function L(ω) are computed using the equations reported in the literature [57].

The imaginary component $\varepsilon_2(\omega)$ represents the phenomenon of light absorption, which occurs when the light frequency exceeds a specific threshold limit [58]. The computed band gap of Cs_2GaAgF_6 double-halide perovskite compound using GGA-PBE approximation is consistent with the absorption onsets of $\epsilon_2(\omega)$ spectra in Fig. 5a. The observed peaks in $\epsilon_2(\omega)$ spectra are attributed to the transition of the electronic states from the valence band to the conduction band. The $\epsilon_2(\omega)$ curves in Fig. 5a attain their maximum at 15.4 eV. Thereafter, the $\epsilon_2(\omega)$ spectra begin to decrease with an increase in energy. The $\varepsilon_1(\omega)$ describes the polarization and dispersion of the light from the lattice [58]. The ε1(ω) spectra in Fig. 5b increase from zero energy and attain a maximum of 3.6 at 5.8 eV. The energy transmission continues until the $\epsilon_1(\omega)$ spectra becomes negative at 15.4–16.6 eV. At this point, the incident photon energies are assumed to be fully attenuated [59], and the Cs_2GaAgF_6 double-halide perovskite compound exhibits metallic behavior [60]. These negative values translate to limited transmission, reflection, and optical energy losses, suggesting a material's suitability as an insulator within this energy range [61]. The zero-frequency limit, ε1(0), also called the static point, is correlated with the refractive index, n(0), as the square root of ε1(ω) at energy (eV) = 0. The static value obtained for the Cs_2GaAgF_6 double-halide perovskite compound is 2.72, as seen in Fig. 5b. The refractive index describes the bending of light traveling through a material. The n(0) value of the Cs_2GaAgF_6 double-halide perovskite compound observed in Fig. 5c is 1.65. The n(ω) spectra in Fig. 5c is observed to be high in the 4.6–15 eV energy regions and thereafter decrease. The α(ω) spectra demonstrate the depth of light of a specific wavelength that can penetrate the material before complete absorption [62]. As shown in Fig. 5d, the α(ω) spectra increase gradually through the visible region and peak in the ultraviolet (UV) region, reaching a maximum at 15.6 eV. The high optical absorption of the Cs_2GaAgF_6 double-halide perovskite compound in the ultraviolet region highlights its potential utility in UV photodetectors [63] and tandem solar cell configurations [64], where UV absorption contributes to the overall device efficiency.

The σ(ω) is directly correlated to the α(ω). As shown in Fig. 6a, the σ(ω) spectra pattern matches that of α(ω) in Fig. 5d. The σ(ω) spectra increase with increasing energy, reaching a maximum of 55,810 S/m in the ultraviolet region at 16.3 eV. These results show that the Cs_2GaAgF_6 double-halide perovskite compound is a good optical conductor that can be used in optoelectronics. The k(ω) describes the amount of absorbed energy by a material. The threshold energy of k(ω) for the Cs_2GaAgF_6 double-halide perovskite compound is determined to be 2.5 eV in Fig. 6b. The k(ω)

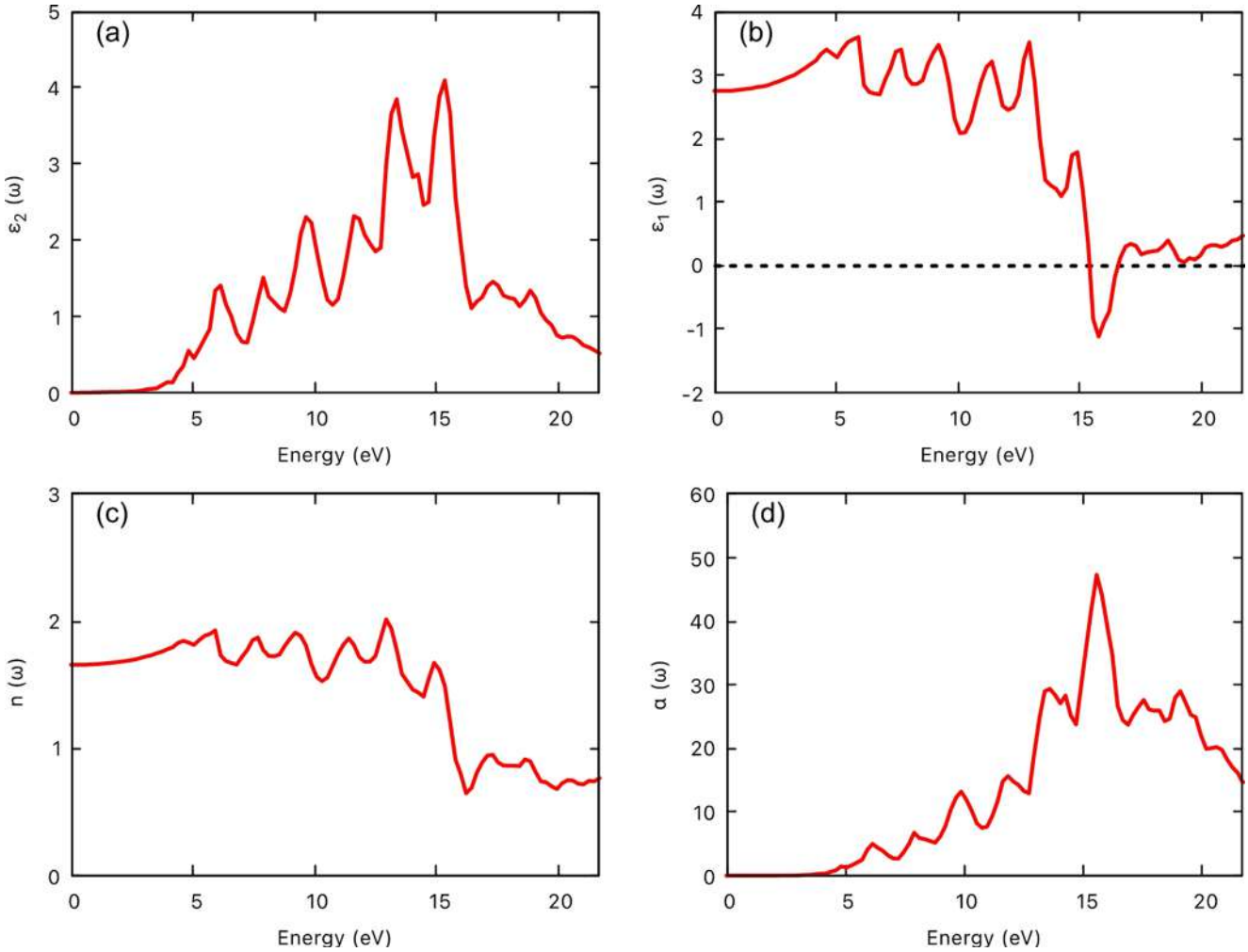

Fig. 5 **a** Imaginary dielectric constant, **b** real dielectric constant, **c**refractive index, and **d** absorption coefficient of the Cs_2GaAgF_6 double-halide perovskite compound

spectra in Fig. 6b increase strongly with increasing energy and attain a maximum in the UV region. This reflects the substantial absorption of the Cs_2GaAgF_6 double-halide perovskite. The R(ω) describes the optical response of the material surface [65]. The static reflectivity R(0) of the Cs_2GaAgF_6 double-halide perovskite compound is 0.06 as seen in Fig. 6c. The R(ω) spectra are observed to increase gradually, attaining a maximum value at 15.9 eV and thereafter gradually decreasing. The L(ω) defines the energy loss by electrons passing through the material [65]. As shown in Fig. 6d, there is a low absorption in the 0–15 eV energy region. Thereafter, a major absorption occurrence is observed. These obtained and observed optical properties are consistent with those reported for other wide band gap halide-based double perovskite compounds [43, 44, 45, 62].

3.5 Thermoelectric Properties

The thermoelectric properties describe the material's ability to generate electrical energy from heat [66]. The transport properties, including Seebeck coefficient (S), electrical conductivity (σ/τ), and electronic thermal conductivity (k_e/τ), were computed using the BoltzTraP code [67] at a temperature (T) ranging from 50 to 800 K (see Fig. 7). The S for Cs_2GaAgF_6 double-halide perovskite compound exhibits a decreasing trend with temperature, starting at 188 μV/K at 50 K and gradually reducing to 149 μV/K at 800 K as observed in Fig. 7a. This behavior aligns with the general trend observed in many thermoelectric materials, where increasing the carrier concentration at higher temperatures reduces the Seebeck coefficient owing to the inverse relationship between S and charge carrier density. The σ/τ in Fig. 7b increases steadily with temperature, reaching 1.35×10^{19} S/m at 800 K. This increase suggests that Cs_2GaAgF_6 follows a semiconductor-like behavior, where

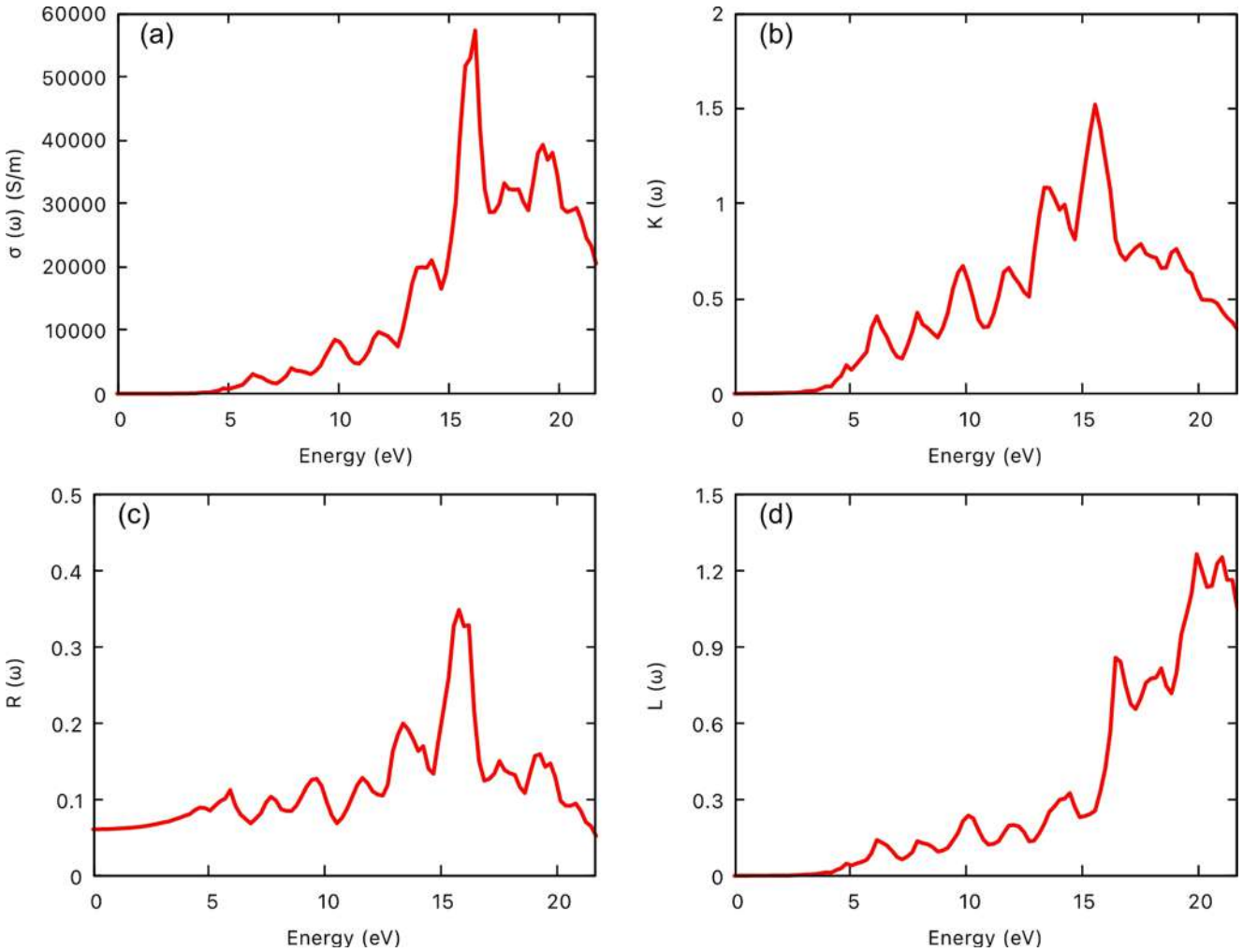

Fig. 6 **a** Optical conductivity, **b** extinction coefficient, **c** reflectivity spectra, and **d** energy loss function of Cs_2GaAgF_6 double-halide perovskite compound

higher temperatures enhance carrier excitation, thus improving conductivity. Such behavior is crucial for an efficient thermoelectric material, as higher conductivity minimizes the Joule heating losses. The k_e/τ in Fig. 7c rises significantly with temperature, from 4.47×10^{12} W/mK at 50 K to 3.28×10^{14} W/mK at 800 K. This increase correlates with the growing electrical conductivity, as dictated by the Wiedemann-Franz law. However, the increasing electronic thermal conductivity should be balanced by a low lattice thermal conductivity (k_l) for optimal thermoelectric performance. The k_l was computed using the phono3py code [68] and the Quantum Espresso code. The k_l shown in Fig. 7d exhibits a decreasing trend with increasing temperature, dropping from 1.46×10^7 W/mK at 50 K to 1.22×10^6 W/mK at 800 K. The obtained k_l values are within a reasonable range as compared to other related double perovskite materials [A_2GeSnF_6 (A=K, Rb, Cs)] whose values have been reported to be in the range 5.53×10^{13} to 0.24×10^{13} W/mKs, 5.83×10^{13} to 0.53×10^{13} W/mKs, and 2.91×10^{13} to 0.122×10^{13} W/mKs, respectively [49]. This reduction indicates enhanced phonon scattering at higher temperatures, a desirable feature of thermoelectric materials for suppressing heat dissipation and improving the figure of merit (ZT). The ZT was calculated from the computed transport properties using Eq. (8) [69].

$$ZT = \frac{S^2 \sigma T}{k_e + k_l} \tag{8}$$

As observed in Fig. 7e, the dimensionless ZT improves with temperature, peaking at 0.739 at approximately 600 K, and maintaining high values thereafter. This peak reflects an optimal operating temperature window around 600 K, where the trade-off between the decreasing Seebeck coefficient, increasing electrical conductivity, and decreasing lattice thermal conductivity yields the optimal thermoelectric efficiency. This highlights the suitability of Cs_2GaAgF_6 for medium-high temperature thermoelectric applications.

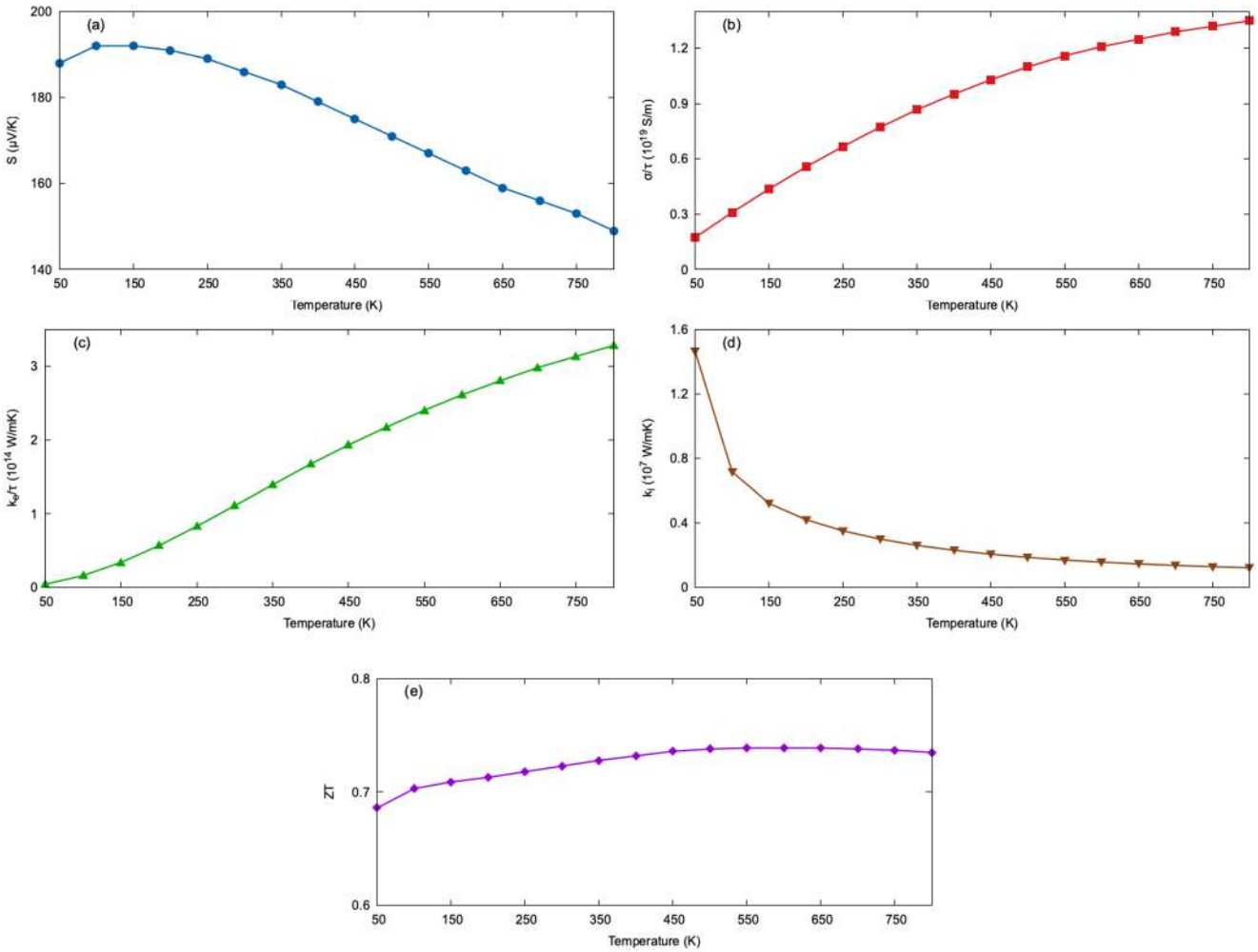

Fig. 7 **a** The Seebeck coefficient (S), **b** electrical conductivity (σ/τ), **c** electronic thermal conductivity (k_e/τ), **d** lattice thermal conductivity (k_l), and **d** figure of merit (ZT) of the Cs_2GaAgF_6 double-halide perovskite compound computed using the GGA-PBE approximation

4 Conclusion

This work examines the structural, electronic, elastic, mechanical, optical, and thermoelectric properties of Cs_2GaAgF_6 double-halide perovskite compound for optoelectronic and thermoelectric applications. The structural, thermodynamic, and mechanical stability of the studied compound is confirmed through nonimaginary phonon frequency modes, negative formation energies, and elastic constants, respectively. The Cs_2GaAgF_6 double-halide perovskite compound is found to be ductile and elastically anisotropic from mechanical and elastic calculations. The wide band gaps ranging from 2.27 eV to 4.62 eV were obtained using different approximation methods. The F2*p* and Ag3*d* states primarily contribute to the formation of the valence band, whereas the Ga2*p*, Ag2*p*, Ga1*s*, and Ag1*s* states significantly influence the formation of the conduction band. Optical absorption bands were observed in the ultraviolet region, which is potentially crucial for optoelectronic applications. Additionally, the Cs_2GaAgF_6 double-halide perovskite compound showed significant thermoelectric performance with a high ZT value of 0.739 at approximately 600 K, indicating its potential as a thermoelectric material. This work thus provides theoretical insights that may guide and motivate future experimental synthesis and characterization of Cs_2GaAgF_6 double-halide perovskite compound.

Acknowledgements The authors acknowledge the University of Nairobi for resources in doing this work and the Centre for High-Performance Computing (CHPC-RSA) for computing resources through account number MATS1321.

Author Contributions M. M.: Project administration, conceptualization, data curation, methodology, formal analysis, validation, original draft writing, review andf editing. R. M.: Funding acquisition, project administration, resources, software, data curation, methodology, formal analysis, validation, review and editing. J. P. K.: Methodology, validation, review and editing. M. N.: Methodology, validation, review and editing. I. M.: Methodology, validation, review and editing. S. W.: Methodology, validation, review and editing. M. Y.: Methodology, validation, review and editing.

Funding The authors did not receive support from any organization for the submitted work.

Data Availability No datasets were generated or analysed during the current study.

Declarations

Conflict of interest The authors have no conflicts of interest to declare that are relevant to the content of this article.

References

1. K. Javan et al., A review of interconnected challenges in the water–energy–food nexus: urban pollution perspective towards sustainable development. Sci. Total Environ. **912**, 169319 (2024). https://doi.org/10.1016/j.scitotenv.2023.169319
2. T.-Z. Ang et al., A comprehensive study of renewable energy sources: classifications, challenges and suggestions. Energy Strateg Rev. **43**, 100939 (2022). https://doi.org/10.1016/j.esr.2022.100939
3. P. Roy et al., Perovskite solar cells: a review of the recent advances. Coatings. **12**(8), 1–24 (2022). https://doi.org/10.3390/coatings12081089
4. J. Zhou et al., Passivating contacts for high-efficiency silicon-based solar cells: from single-junction to tandem architecture. Nano Energy. **92** (2022). https://doi.org/10.1016/j.nanoen.2021.106712
5. F. Cao, L. Bian, L. Li, Perovskite solar cells with high-efficiency exceeding 25%: a review. Energy Mater. Devices. **2**(1), 9370018 (2024). https://doi.org/10.26599/EMD.2024.9370018
6. M. Habibi et al., Progress in emerging solution-processed thin film solar cells—part II: perovskite solar cells. Renew. Sustain. Energy Rev. **62**, 1012–1031 (2016). https://doi.org/10.1016/j.rser.2016.05.042
7. C. Zhao et al., Stabilization of highly efficient perovskite solar cells with a tailored supramolecular interface. Nat. Commun. **15**(1), 7139 (2024). https://doi.org/10.1038/s41467-024-51550-z
8. M. Noman, Z. Khan, S.T. Jan, A comprehensive review on the advancements and challenges in perovskite solar cell technology. RSC Adv. **14**(8), 5085–5131 (2024). https://doi.org/10.1039/D3RA07518D
9. S. Charef, A. Assali, A. Boukortt, Optoelectronic and thermoelectric properties of novel double halide perovskites Na_2AgAsX_6 (X = Cl, Br) for efficient green solar cells. Mater. Today Commun. **38**, 108065 (2024). https://doi.org/10.1016/j.mtcomm.2024.108065
10. A. Mera et al., Exploring the physical properties of Rb_2TlSbM_6 (M = Cl, Br) inorganic halide perovskites for solar cell applications: a dFT study. Inorg. Chem. Commun. **165**, 112528 (2024). https://doi.org/10.1016/j.inoche.2024.112528
11. M. Kibbou et al., Designing new halide double perovskite materials Rb2AgGaX6 (X: Br, Cl) with direct band gaps and high power conversion efficiency. J. Solid State Chem. **317**, 123698 (2023). https://doi.org/10.1016/j.jssc.2022.123698
12. T. Tang, Y. Tang, A first principle comparison of arsenic-based double halide perovskite materials for photovoltaic and optoelectronic application. J. Solid State Chem. **316**, 123557 (2022). https://doi.org/10.1016/j.jssc.2022.123557
13. M. Kibbou et al., Computational insights into the superior efficiency of Cs2AgGa(Cl,Br)6 double halide perovskite solar cells. Mater. Chem. Phys. **294**, 126978 (2023). https://doi.org/10.1016/j.matchemphys.2022.126978
14. Z. Zhang et al., Hydrogenated Cs2AgBiBr6 for significantly improved efficiency of lead-free inorganic double perovskite solar cell. Nat. Commun. **13**(1), 3397 (2022). https://doi.org/10.1038/s41467-022-31016-w
15. P. Honenberg, W. Kohn, I.E. Gas, Phys. Rev. **136**(3B), 1–8 (1964). https://doi.org/10.1007/BF01198136
16. P. Giannozzi et al., QUANTUM ESPRESSO: a modular and open-source software project for quantum simulations of materials. J. Phys. Condens. Matter. **21**(39), 395502 (2009). https://doi.org/10.1088/0953-8984/21/39/395502
17. D. Vanderbilt, Soft self-consistent pseudopotentials in a generalized eigenvalue formalism. Phys. Rev. B **41**(11), 7892–7895 (1990). https://doi.org/10.1103/PhysRevB.41.7892
18. D.R. Hamann, M. Schlüter, C. Chiang, N.-C. Pseudopotentials. Phys. Rev. Lett. **43**(20), 1494–1497 (1979). https://doi.org/10.1103/PhysRevLett.43.1494
19. P. Ziesche, S. Kurth, J.P. Perdew, Density functionals from LDA to GGA. Comput. Mater. Sci. **11**(2), 122–127 (1998). https://doi.org/10.1016/S0927-0256(97)00206-1
20. J.P. Perdew, K. Burke, M. Ernzerhof, Generalized gradient approximation made simple. Phys. Rev. Lett. **77**(18), 3865–3868 (1996). https://doi.org/10.1103/PhysRevLett.77.3865
21. Z. Wu, R.E. Cohen, More accurate generalized gradient approximation for solids. Phys. Rev. B - Condens. Matter Mater. Phys. **73**(23), 2–7 (2006). https://doi.org/10.1103/PhysRevB.73.235116
22. J.W. Furness et al., Accurate and numerically efficient r2SCAN meta-generalized gradeneralized gradient approximation. J. Phys. Chem. Lett. **11**(19), 8208–8215 (2020). https://doi.org/10.1021/acs.jpclett.0c02405
23. Z. Yang et al., More realistic band gaps from meta-generalized gradient approximations: only in a generalized Kohn-Sham scheme. Phys. Rev. B **93**(20), 205205 (2016). https://doi.org/10.1103/PhysRevB.93.205205
24. J. Sun, A. Ruzsinszky, J.P. Perdew, Strongly constrained and appropriately normed semilocal density functional. Phys. Rev. Lett. **115**(3), 36402 (2015). https://doi.org/10.1103/PhysRevLett.115.036402
25. D. Koller, F. Tran, P. Blaha, Improving the modified Becke-Johnson exchange potential. Phys. Rev. B - Condens. Matter Mater. Phys. **85**(15), 1–8 (2012). https://doi.org/10.1103/PhysRevB.85.155109
26. T. Atsue, I.B. Ogunniranye, O.E. Oyewande, Investigation of material properties of halide mixed lead - free double perovskite for optoelectronic applications using first-principles study. Mater. Sci. Semicond. Process. **133**, 105963 (2021). https://doi.org/10.1016/j.mssp.2021.105963
27. S. Bağci et al., Electronic and phonon properties of BX (110) (X = P, as, and Sb) and BeY (110) (Y = S, Se, and Te) surfaces. Phys. Rev. B Condens. Matter Mater. Phys. **79**(12), 1–13 (2009). https://doi.org/10.1103/PhysRevB.79.125326
28. O. Isayev et al., Universal fragment descriptors for predicting properties of inorganic crystals. Nat. Commun. **8**, 1–12 (2017). https://doi.org/10.1038/ncomms15679
29. F. Legrain et al., How chemical composition alone can predict vibrational free energies and entropies of solids. Chem. Mater. **29**(15), 6220–6227 (2017). https://doi.org/10.1021/acs.chemmater.7b00789
30. V. Stanev et al., Machine learning modeling of superconducting critical temperature. Npj Comput. Mater. **4**(1) (2018). https://doi.org/10.1038/s41524-018-0085-8
31. E. Gossett et al., AFLOW-ML: A restful API for machine-learning predictions of materials properties. Comput. Mater. Sci. **152**, 134–145 (2018). https://doi.org/10.1016/j.commatsci.2018.03.075
32. R. Musembi et al., Analysis of Na2CuP ternary semiconductor compound for optoelectronic application by first-principles

methods using GGA and mGGA functionals. Comput. Condens. Matter. **40** (2024). https://doi.org/10.1016/j.cocom.2024.e00927. e00927
33. T.M. Project, Materials data on Cs2GaAgF6 by materials project. United States. (2020). https://doi.org/10.17188/1725173
34. G.S. Manyali, R. Warmbier, A. Quandt, Computational study of the structural, electronic and optical properties of M2N2(NH): M=C, Si, Ge, Sn. Comput. Mater. Sci. **79**, 710–714 (2013). https://doi.org/10.1016/j.commatsci.2013.07.038
35. M.N.H. Liton et al., Unlocking the mechanical, thermodynamic and thermoelectric properties of NaSbS2: A DFT scheme. Heliyon. **11**(1) (2025). https://doi.org/10.1016/j.heliyon.2024.e41220. e41220
36. R. Musembi, M. Mbilo, Computational study on structural, elastic, mechanical and optical properties of K2AgAs ternary semiconductor compound. AIP Adv. **13**(11), 115218 (2023). https://doi.org/10.1063/5.0170089
37. S. Baroni, P. Giannozzi, E. Isaev, Density-functional perturbation theory for quasi-harmonic calculations. Theor. Comput. Methods Miner. Phys. Geophys. Appl. 71(1985), 39–58 (2018) https://doi.org/10.2138/rmg.2010.71.3
38. Ş. Uğur et al., DFT analysis of the electronic, optical, phonon, elastic, and mechanical features of ternary Rb2XS3 (X=Si, Ge, Sn) chalcogenides. Opt. Quantum Electron. **56**(7), 1–17 (2024). https://doi.org/10.1007/s11082-024-07046-7
39. N. Pandey, N. Neelu, S. Chakrabarti, Room temperature synthesis of double perovskite Cs2AlBiCl6 for photovoltaic applications. Opt. Mater. (Amst). **137**, 113570 (2023). https://doi.org/10.1016/j.optmat.2023.113570
40. R.S. Lamba et al., Extending the absorption of Cs2AgBiCl6 double perovskite to the near infra-red region by copper doping. J. Mater. Chem. C **12**(13), 4792–4799 (2024). https://doi.org/10.1039/D3TC03567K
41. D. Abdullah, D.C. Gupta, Analyzing the structural, optoelectronic, and thermoelectric properties of InGeX3 (X=Br) perovskites via DFT computations. Sci. Rep. **14**(1), 23575 (2024). https://doi.org/10.1038/s41598-024-72745-w
42. M. Mbilo, R. Musembi, First principles calculation to investigate the structural, electronic, elastic, mechanical, and optical properties of K2NiP2 ternary compound. AIP Adv. **12**, 105018 (2022). https://doi.org/10.1063/5.0118809
43. S. Shakeel et al., DFT analysis of elastic and optoelectronic properties of Cs2NaXCl6 (X=In, La, Sc, Y) double perovskite compounds. Mater. Chem. Phys. **324**, 129683 (2024). https://doi.org/10.1016/j.matchemphys.2024.129683
44. D. Abdullah, D.C. Gupta, Understanding the mechanical, optoelectronic, and thermoelectric properties of lead-free silver based perovskites Cs2YAgX6 (X=Cl, Br, I): A computational study. Comput. Condens. Matter. **40** (2024). https://doi.org/10.1016/j.cocom.2024.e00924. e00924
45. S.H. Shah et al., Comprehensive study of structural, elastic, electronic, optical, and thermoelectric properties of Rb2NaTlZ6 (Z=Cl, Br, and I) by DFT. Mater. Sci. Semicond. Process. **178**, 108400 (2024). https://doi.org/10.1016/j.mssp.2024.108400
46. S. Yuvaraja et al., Wide bandgap semiconductor-based integrated circuits. Chip. **2**(4), 100072 (2023). https://doi.org/10.1016/j.chip.2023.100072
47. F. Mouhat, F.X. Coudert, Necessary and sufficient elastic stability conditions in various crystal systems. Phys. Rev. B Condens. Matter Mater. Phys. **90**(22), 1–4 (2014). https://doi.org/10.1103/PhysRevB.90.224104
48. R. Hill, The elastic behaviour of a crystalline aggregate. Proc. Phys. Soc. Sect. A 65, 349–354 (1952)
49. D. Abdullah, D.C. Gupta, Probing the opto-electronic, phonon spectrum, and thermoelectric properties of lead-free fluoride perovskites A2GeSnF6 (A=K, Rb, Cs) for energy harvesting devices. Sci. Rep. **14**(1), 1–14 (2024). https://doi.org/10.1038/s41598-024-61210-3
50. D. Hong et al., The structural, mechanical and electronic properties of NbXSi (X=Fe, Co, Ni, Ru, Rh, Pd, Os, Ir and Pt) compounds from first-principles calculations. Mater. Chem. Phys. **259**, 124029 (2021). https://doi.org/10.1016/j.matchemphys.2020.124029
51. M.I. Kholil, M.T.H. Bhuiyan, Electronic, elastic, vibrational and superconducting properties of a ternary superconductors LaIrP (P=P, As): insights from DFT. Solid State Commun. **322**, 114053 (2020). https://doi.org/10.1016/j.ssc.2020.114053
52. J. Fu, F. Bernard, S. Kamali-Bernard, First-principles calculations of typical anisotropic cubic and hexagonal structures and homogenized moduli estimation based on the Y-parameter: application to CaO, MgO, CH and calcite CaCO3. J. Phys. Chem. Solids. **101**, 74–89 (2017). https://doi.org/10.1016/j.jpcs.2016.10.010
53. R. Gaillac, P. Pullumbi, F.X. Coudert, An open-source online application for analysis and visualization of elastic tensors. J. Phys. Condens. Matter. **28**(27) (2016). https://doi.org/10.1088/0953-8984/28/27/275201
54. M.H. Sahafi, E. Cholaki, A.I. Bashir, First-principles calculations to investigate phonon dispersion, mechanical, elastic anisotropy and thermodynamic properties of an actinide-pnictide ceramic at high pressures/temperatures. Results Phys. **58**, 107495 (2024). https://doi.org/10.1016/j.rinp.2024.107495
55. R. Bhattacharjee, S. Chattopadhyaya, Effects of barium (Ba) doping on structural, electronic and optical properties of binary strontium chalcogenide semiconductor compounds - a theoretical investigation using DFT based FP-LAPW approach. Mater. Chem. Phys. **199**, 295–312 (2017). https://doi.org/10.1016/j.matchemphys.2017.06.057
56. A. Srivastava et al., Structural, electronic and optical properties of Ag2MgSn(S/Se)4 quaternary chalcogenides as solar cell absorber layer: an ab-initio study. Sol Energy. **209**, 206–213 (2020). https://doi.org/10.1016/j.solener.2020.08.094
57. S. Azam et al., DFT study of the electronic and optical properties of ternary chalcogenides AlX2Te4. Mater. Res. Express. **6**(11), 116314 (2019). https://doi.org/10.1088/2053-1591/ab4b81
58. T.I. Al-Muhimeed et al., First principle study of optoelectronic and mechanical properties of lead-free double perovskites Cs 2 sex 6 (X=Cl, Br, I). J. Taibah Univ. Sci. **16**(1), 155–162 (2022). https://doi.org/10.1080/16583655.2022.2035927
59. G. Murtaza, I. Ahmad, First principle study of the structural and optoelectronic properties of cubic perovskites CsPbM3 (M=Cl, Br, I). Phys. B Condens. Matter. **406**(17), 3222–3229 (2011). https://doi.org/10.1016/j.physb.2011.05.028
60. M.S. Khan et al., Insights into the optoelectronic, thermodynamic, and thermoelectric properties of novel BaYCuX3 (X=Se, Te) semiconductors from first-principles investigation. Mater. Sci. Semicond. Process. **181**, 108627 (2024). https://doi.org/10.1016/j.mssp.2024.108627
61. A. Ayyaz et al., Influence of alkali metal cation modifications on physical characteristics of double perovskites Rb2XTlBr6 (X=Li, Na, K): First-principles study for solar energy and thermoelectric applications. Phys. B Condens. Matter. **690**, 416245 (2024). https://doi.org/10.1016/j.physb.2024.416245
62. M.S. Khan, E. Structure et al., Optical and thermoelectric properties of novel Rb 2 XAgF 6 (X=Ga and In) halide-based perovskites. J. Inorg. Organomet. Polym. Mater. **6**, 1–13 (2025). https://doi.org/10.1007/s10904-024-03579-2
63. F. Cao et al., Wide bandgap semiconductors for ultraviolet photodetectors: approaches, applications, and prospects. Research. **7**, 1–23 (2024). https://doi.org/10.34133/research.0385
64. A.J. Ramadan et al., Methylammonium-free wide-bandgap metal halide perovskites for tandem photovoltaics. Nat. Rev. Mater.

8(12), 822–838 (2023). https://doi.org/10.1038/s41578-023-00610-9
65. M.S. Yaseen et al., First-principles study of electronic and optical properties of ternary compounds AuBX2 (X=S, Se, Te) and AuMTe2 (M=Al, in, Ga). Solid State Sci. **111**, 106508 (2021). https://doi.org/10.1016/j.solidstatesciences.2020.106508
66. D. Abdullah, D.C. Gupta, DFT simulations of the elastic, optoelectronic, and thermoelectric attributes of AOsCl3 (A=K, Rb), a robust and environmentally friendly perovskites for green energy implications. Sci. Rep. **14**(1), 26168 (2024). https://doi.org/10.1038/s41598-024-73412-w
67. G.K.H. Madsen, D.J. Singh, BoltzTraP. A code for calculating band-structure dependent quantities. Comput. Phys. Commun. **175**(1), 67–71 (2006). https://doi.org/10.1016/j.cpc.2006.03.007
68. A. Togo et al., Implementation strategies in phonopy and phono3py. J. Phys. Condens. Matter. **35**, 353001 (2023). https://doi.org/10.1088/1361-648X/acd831
69. S. Irfan, Z. Yan, S.B. Khan, Advancements in thermoelectric materials: A comprehensive review. Mater. Sci. Energy Technol. **7**, 349–373 (2024). https://doi.org/10.1016/j.mset.2024.06.002